

pubs.acs.org/JPCB Article

Predicting the Geometry of Core—Shell Structures: How a Shape Changes with Constant Added Thickness

Christopher D. Gale* and Nancy E. Levinger*



Cite This: J. Phys. Chem. B 2024, 128, 1317–1324



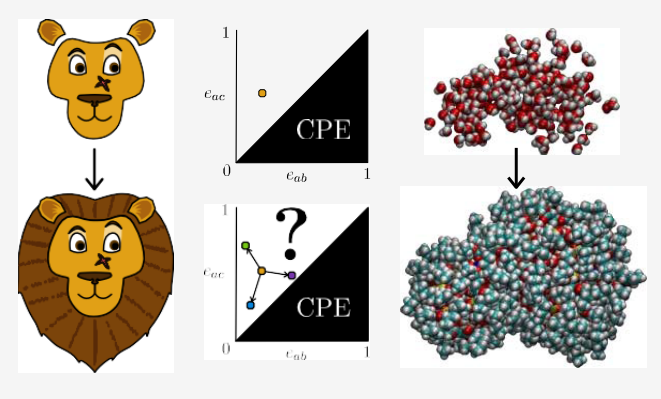
ACCESS I

Metrics & More

Article Recommendations

Supporting Information

ABSTRACT: The core—shell assembly motif is ubiquitous in chemistry. While the most obvious examples are core/shell-type nanoparticles, many other examples exist. The shape of the core/shell constructs is poorly understood, making it impossible to separate chemical effects from geometric effects. Here, we create a model for the core/shell construct and develop proof for how the eccentricity is expected to change as a function of the shell. We find that the addition of a constant thickness shell always creates a relatively more spherical shape for all shapes covered by our model unless the shape is already spherical or has some underlying radial symmetry. We apply this work to simulated AOT reverse micelles and demonstrate that it is remarkably successful at explaining the observed shapes of the chemical systems. We identify the three



specific cases where the model breaks down and how this impacts eccentricity.

1. INTRODUCTION

Systems adopting a core/shell motif, where an external layer wraps an interior core, are prevalent in chemistry, biology, physics, and materials science. Although core/shell nanoparticles are perhaps the most obvious example of this phenomenon and have applications in many of the fields identified, 1-4 this motif is observed in many other contexts. 5-12 A surfactant layer that stabilizes many nanoparticles presents a "shell" layer around the nanoparticle "core." Soft materials or supramolecular assemblies, such as micelles 14,15 or reverse micelles, fall into this pattern too; a micelle essentially comprises a core coated with a surfactant layer as a shell around it. Cellular organelles may also appear as core/shell systems in which the interior of the organelle is the core, while the boundary, often a lipid bilayer, constitutes the shell.¹⁶ Even solute/solvent interactions may be represented as core/shell structures, where the solute occupies a void in the solvent considered the core—and the solvation shells act as their namesake: the shell.^{9,10}

In many of these scenarios, the shape of the core/shell assembly is important to the function of the particle. ^{3,14,17-19} Nanoparticles may form any number of shapes, and control of nanoparticle shapes is often a highly prized synthetic target. ²⁰⁻²⁵ Controlling shape may lead to consistent characteristics that enable properties to be tuned. ^{24,25} In solute physics, the shape of the cavity a solute occupies within a solvent is vital to understanding the solute—solvent interactions involved. ^{9,10,12,26} This is especially true for proteins, where the shape is both extremely complex and vital to their function. ^{17,19} The first solvation shell around the particles or macromolecules itself may

also be of great interest. For example, dynamic light scattering—a ubiquitous method for measuring particle size—tracks the hydrodynamic size of the particle and, therefore, includes not just the particle but also what diffuses with the particle.²⁷

In all of these cases, little is known about how the interior and exterior shapes of core/shell-type objects are related. Solid nanoparticles can be observed using techniques such as electron microscopy. ^{1,16,20–25,28} Similarly, protein structures, and thus their shapes, may be experimentally determined using, for example, X-ray diffraction, NMR, and cryo-electron microscopy. 29-31 However, for both nanoparticles and proteins, we are limited to measurements of shape only after fully determining their structure with very little a priori understanding of the shape. This strictly post hoc view precludes a broader understanding of the shape and the impact of a shell. For instance, we have very little understanding of how the shape of solvation shells around a protein change relative to the shape of the protein itself, even though this is critical to understanding protein behavior in solution without a bulky and difficult QM/ MM calculation.³² Similarly, there is no broad understanding of how a shell will impact the behavior of a nanoparticle outside of extensive trial-and-error work. The difficulty in all of these

Received: November 20, 2023
Revised: January 14, 2024
Accepted: January 16, 2024
Published: January 30, 2024





scenarios is that the shapes vary wildly, spanning everything from highly regular geometric shapes, such as spherical or cubic nanoparticles, to the irregular shapes encountered in protein structures and reverse micelles.

We have recently presented a method to quantify amorphous shapes, which we demonstrated on sodium bis(2-ethylhexyl) sulfosuccinate (AOT) reverse micelles simulated using molecular dynamics.³³ A basic representation of an AOT reverse micelle is shown in Figure 1a. Here, the water acts as the core of

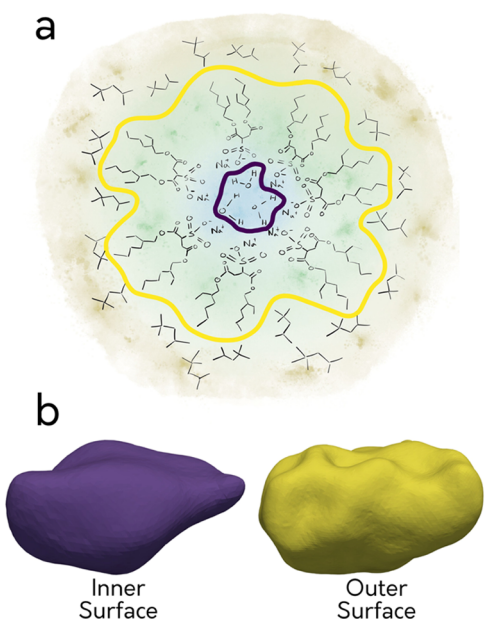


Figure 1. Three representations of AOT reverse micelles. (a) Cartoon of an AOT reverse micelle, illustrating its basic construction. Water is shown on a blue background at the center, AOT is shown on a green background at the interface, and both are dispersed in an isooctane phase, on a yellow background. (b) Inner, water-only surface (purple) and outer, water + AOT + sodium surface (yellow) of our reverse micelle from a random frame in the simulation, obtained by the Willard—Chandler interface-finding algorithm. ^{38,39} The surfaces are not shown to scale to highlight the relative shapes of the surfaces.

the particle, while the AOT surfactant layer acts as the shell. Amorphous and constantly changing their shapes, AOT reverse micelles are only roughly ellipsoidal at any instant in time. 33-37 Molecular dynamics simulations provide an opportunity to study these shapes in frame-by-frame detail and explore how the shape evolves. Here, we use the atomistic detail of the simulation to break the reverse micelle into multiple surfaces and study how the shape evolves throughout the micelle by studying the changes between the water core and the AOT/oil interface. Figure 1 presents a basic characteristic of the reverse micelle we are simulating, as well as the inner, water-pool-only surface and the outer, AOT+water+Na+ surface of the reverse micelle from an arbitrary frame in our simulation. Figure 1b demonstrates that although the reverse micelles are clearly nonspherical, further characterization is difficult. It may be easy to visually identify that the two surfaces are different, but it is much more difficult to identify the specific characteristics that comprise this difference. For example, the authors differed on which of these two images were more spherical from Figure 1b alone. The outer surface is much rougher and has many divots not present in the inner surface, but the impact of these features on the shape is not immediately clear. And, of course, the only way to extend those

observations to other instances is to directly observe each of those other instances, which is not only subjective but also quickly becomes a daunting and labor-intensive task. Therefore, AOT reverse micelles are an excellent model system for studying how shape changes as a function of the shell in a core/shell construction in the extreme of a fluctuating, amorphous, poorly described shape. We will use this simulation as both a test and an example for the general model of shape developed in this work.

This conundrum, where we can clearly see the shapes but lack a good way to quantitatively describe or predict them, is at the heart of this work. Although several methods exist for characterizing shapes in various ways, it is not understood how these measures change as a shell around the shape is created, as seen in many different fields of chemistry. The change in the shape could be computed numerically from most simulations, but without a broader understanding of this behavior, it is still unknown whether the computed values reflect the system behaving as expected or not, and whatever results are found cannot be applied to experimental work outside of the limited case simulated. Here, we address the issue of the shape characteristics of a core/shell construction by developing a model and proving that the shape will become more spherical as a shell "grows" around a shape, developing a broad understanding that can be applied to any core/shell motif.

2. METHODS

The data presented here is from a simulation detailed in our previous work, 33 except that the production run was altered to run for 1 μ s in total with a 2 fs step size, but otherwise identical and starting from the same equilibration. Briefly, the $w_0 = 5$ reverse micelle, with an aggregation number of 42, was packed using PACKMOL.⁴⁰ The system's potential energy was minimized to avoid bad contacts by the steepest descent algorithm. The system was equilibrated for 10 ns in total using a series of heavy-atom position restraints detailed in our previous work.33 Equilibration was carried out using the V-rescale thermostat⁴¹ and the Berendsen barostat.⁴² Production was carried out with the Nose-Hoover thermostat and Parrinello-Rahman barostat. 43-46 Both equilibration and production were held at 298 K and 1 bar and used the NPT ensemble. The production trajectory recorded positions and velocities every 8 ps. The simulation used Abel's parameters for AOT reverse micelles, which are based on the CHARMM force field and use TIP3P water. 34,47,48 All simulations used the 2019 series of the GROMACS package. 49-52 GROMACS was used to compute the apparent semiaxes for both surfaces from the simulation.

3. MODEL

We use coordinate-pair eccentricity (CPE) as the basis for determining shape in this work, ³³ although there are numerous other ways to characterize the sphericity of an object, ^{53–55} and several more that specifically classify the object as an ellipsoid of some form. ^{34,36,37,56} All of these methods are based on the moments of inertia and function essentially the same way, such that our findings can be readily translated into any other metric, but the mathematical proof underpinning our findings is dramatically simplified by the symmetry of CPE. CPE is defined

$$e_{ab} = \sqrt{1 - \frac{b^2}{a^2}}, \ a \ge b \ge c$$

$$e_{ac} = \sqrt{1 - \frac{c^2}{a^2}}$$
(1)

where a, b, and c are the semiaxes of the ellipsoid that has the same principal moments of inertia as the object being characterized, e.g., an AOT reverse micelle. CPE is a simple extension of the traditional eccentricity metric. 34,37 The extended CPE values provide a full and accurate characterization of a 3D shape.³³ For highly regular ellipsoids, the values of e_{ab} and e_{ac} can be easily determined. For example, a sphere is defined such that a = b = c, so both e_{ab} and e_{ac} are 0. A prolate ellipsoid, which is a long, thin, "cigar-shaped" object, is defined such that a > b = c, so $e_{ab} = e_{ac} \neq 0$. An oblate ellipsoid, which is a short, fat object like the stereotypical "flying saucer" UFO, is defined as a = b > c, so that e_{ab} is 0 and 0 < $e_{ac} \le 1$. Less regular shapes will have e_{ab} and e_{ac} values that vary from 0 to 1. By convention, the semiaxes are labeled such that $a \ge b \ge c$. CPE values below the line y = x would violate this convention and cannot be observed, so we black out this space in the plot as a visual reminder. Figure 2 provides two graphical representations of CPE; Figure 2a illustrates how the CPE space relates to the oblate/prolate character of the shape. Figure 2b illustrates how the CPE space relates to the sphericity of the shape. Figure 2c is provided for reference to demonstrate the observed shape of the simulated AOT reverse micelles. They are generally nonspherical and tend to be more oblate than prolate with a probability ratio of about 2:1. The division between roughly oblate and roughly prolate shapes is not symmetric, and so a divider line is shown in all plots to aid in determining the division between oblate and prolate. A derivation of this line is provided in the SI Section S11.

In this model, we use an arbitrary shape-e.g., a sphere, cylinder, rectangular prism, etc.—subject only to the conditions that the shape's (principal) moments of inertia can be computed analytically with a linear equation, and the shape is a topological ball, meaning that it does not have a hole, like a torus (see SI Section S4 for more details). Each shape model has its own set of measures. For example, a sphere has a single radius, a cylinder has a radius and a length, and a rectangular prism has a length, a width, and a height. Our model is general and works with all of these examples, even though their measures vary. Throughout the rest of the paper, we refer to all of these measures collectively as "measures of shape" to generalize the various names typically given to these measures. To study how the shape changes as a function of the shell, we increase all measures of shape by a constant, t, to create a "shell" in our model around the initially chosen shape. Figure 3 shows a diagram representation of this model for a cylindrical shape. Here, the yellow "hairs" provide a visual representation of the constant thickness, t, added to the cylinder to produce the outer surface (purple). Although the inner and outer surfaces are geometrically similar objects, their shape properties are not guaranteed to remain the same.

A constant increase in the measures of shape, like that shown in Figure 3, models the typical core—shell motif observed in chemistry well. The shell is constructed by adding a layer of constant thickness, such as the layer of AOT surfactants in our reverse micelles or a noble metal shell grown on a nanoparticle. Using this model, we have developed a proof determining whether and how the CPE changes with the addition of a constant thickness shell. The full proof is provided in the SI. The

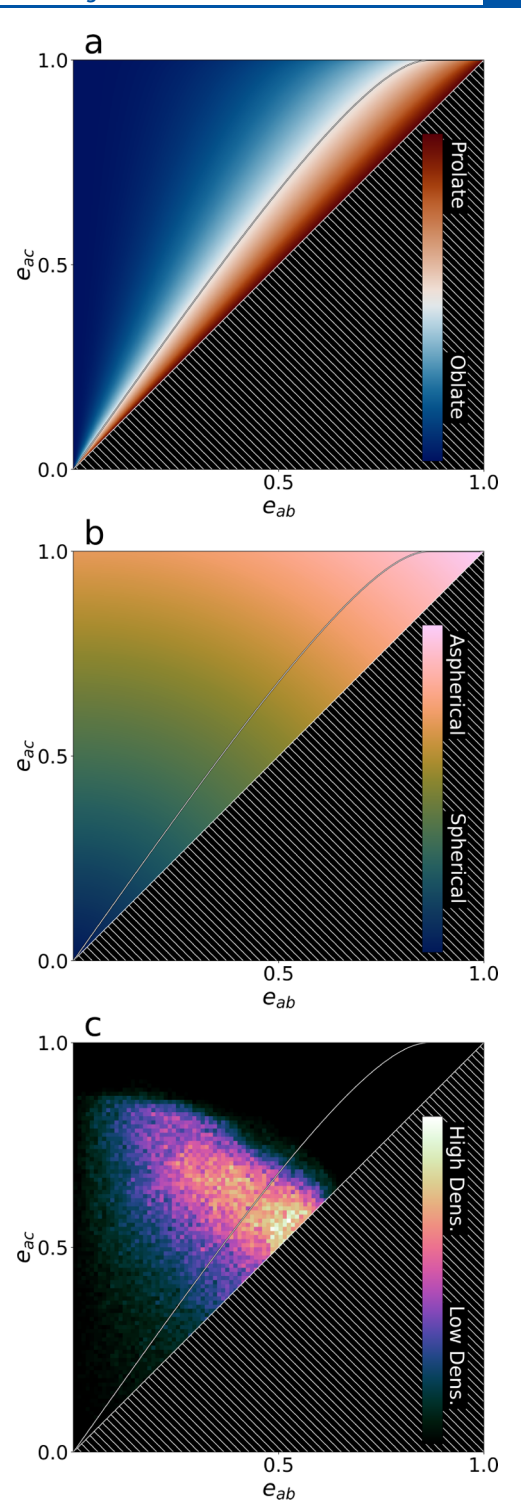


Figure 2. (a) An illustration of the meaning of CPE in terms of how oblate versus how prolate the shape is divided by the curve centered between the regions. (b) Illustration of the meaning of CPE in terms of the sphericity or asphericity of the shape. (c) Observed CPE of the inner surface of the reverse micelle averaged over all times. Brighter-colored areas were observed more frequently. As shown in panel (a), the curve represents the divider between oblate and prolate shapes.

proof first determines whether the shape, as measured by CPE, can remain the same when all measures of shape are increased by a constant thickness. While there is slightly more nuance to our findings, which can be found in SI Section S8, we generally

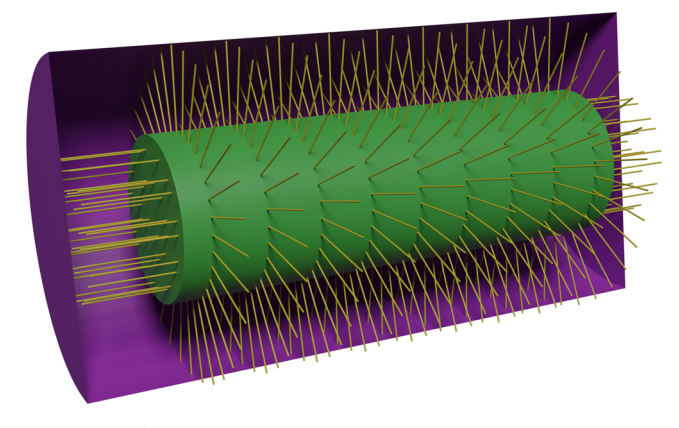


Figure 3. (a) Green cylinder represents the core, while the purple cylinder represents the shell (shown as a cutaway). The "hairs" shown in yellow represent the additional thickness added to the measures of the shape of the core cylinder to create the shell cylinder. This is why the hairs are oriented as shown: extending radial around the length to extend the radius and normal along the flat ends to extend the length.

demonstrate that the shape will change unless the shape is already spherical or a perfectly oblate ellipsoid.

4. RESULTS AND DISCUSSION

Figure 4 compares the difference in CPE between the inner and outer surfaces of the AOT reverse micelle from our simulation,

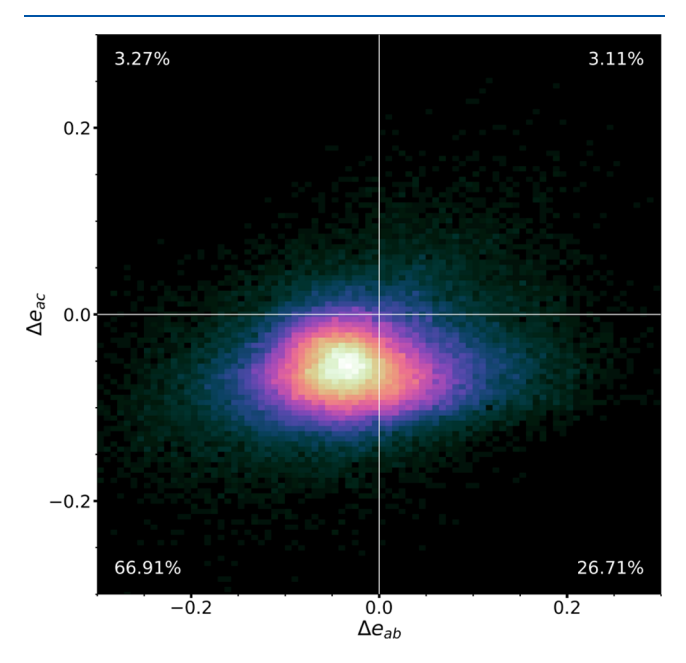


Figure 4. Change in CPE between the inner and outer surfaces over the course of a $1\,\mu s$ simulation, plotted as a heatmap. The brighter the color, the more often those values were observed in the simulation. The colors are assigned based on a power-law to give greater visibility to the low probability values of Δ CPE. Percentages indicate the percentage of frames found in each quadrant.

such as those shown in Figure 1b. The difference is defined as the CPE of the outer surface (AOT+water+Na⁺) minus the CPE of the inner surface (water only), so that negative values indicate that the outer surface is comparatively more spherical in the direction of the given axis. Most of the points (\sim 67%) shown in Figure 4 appear in the third quadrant, where both $\Delta e_{ab} < 0$ and $\Delta e_{ac} < 0$. This indicates that the majority of the time, the outer

surface is relatively more spherical than the inner surface. However, even though most of the points lie in the third quadrant, there are still points in all three of the other quadrants, indicating that both e_{ac} and e_{ab} sometimes vary in opposite directions from each other, and sometimes, the outer surface is less spherical than the inner water pool. The distribution also has a notable skew in the horizontal direction. It is impossible to know from these data alone which parts arise from the unique situation of AOT reverse micelles and which are due simply to the geometry of the core/shell construction of the ensemble.

This leaves the larger question of how the CPE is expected to change with added thickness. In SI Section S9, we demonstrate that it must always fall until it becomes spherical ($e_{ab} = e_{ac} = 0$) in the limit of an infinitely large added thickness. The limit is fairly easy to demonstrate. Imagine synthesizing a core-shell-type nanoparticle where the core nanoparticle is well described as an ellipsoid, with semiaxes of 1, 5, and 10 nm, respectively. The shell-forming reaction is allowed to proceed for far too long, perhaps because a researcher forgot that they had an experiment running, depositing 1 μ m of material uniformly on the initial particle. The resulting semiaxes for the core/shell particle will now be 1.001, 1.005, and 1.010 μ m. In this case, the particle is spherical for all practical purposes. The initial values become effectively meaningless, and all of the outer surface's measures of shape will become equivalent as the added constant, t, grows to infinity. This argument is a chemistry-specific application of Minkowski sums and demonstrates the general idea of our proof exceptionally well.⁵⁷ A formal description of Minkowski sums and their application to this work are provided in SI Section S6.

The fact that an arbitrary shape becomes relatively more spherical as the shell grows has implications for a wide variety of applications, such as solution thermodynamics, for these core/ shell motif systems. Solely because of the geometry of growing a shell, the relatively more spherical shell minimizes its surfacearea-to-volume ratio, thereby also minimizing the free energy of the interface. This suggests that solution properties of both nanomaterials and soft materials can be intelligently modified simply by changing the construction of the material, e.g., by changing the nonpolar tail length of a nanoparticle capping agent. It is important to note that the model presented here is independent of the thermodynamics of the system. A chemical system will find the shape that minimizes free energy, such as is observed in the equilibrium shape of crystals.⁵⁸ However, the work we present is purely geometric and, therefore, remains true in both equilibrium and nonequilibrium situations.

Our model also has implications for shape-dependent measurements, such as dynamic light scattering. This is a common technique for measuring the size of small (1-1000 nm) particles based on their diffusion through a liquid medium. 59,60 Autocorrelation of the light scattered by particles reveals the particle size using the Stokes–Einstein equation, which implicitly assumes a sphere. ^{61,62} Dynamic light scattering measures the hydrodynamic radius rather than the strict particle radius, that is, the apparent radius a spherical particle would need to match the diffusion speed of the real particle. This includes shape effects but also any solvent molecules, capping molecules, or coronae dragged along with the particle being studied due to viscosity or other factors, such as a protein corona on an *in vivo* nanoparticle.⁶⁰ The model we present here shows that the assumption of a spherical particle inherent in the Stokes-Einstein equation is more accurate when considering the hydrodynamic shape, which includes a shell of solvent molecules dragged by viscous forces, than the shape of the

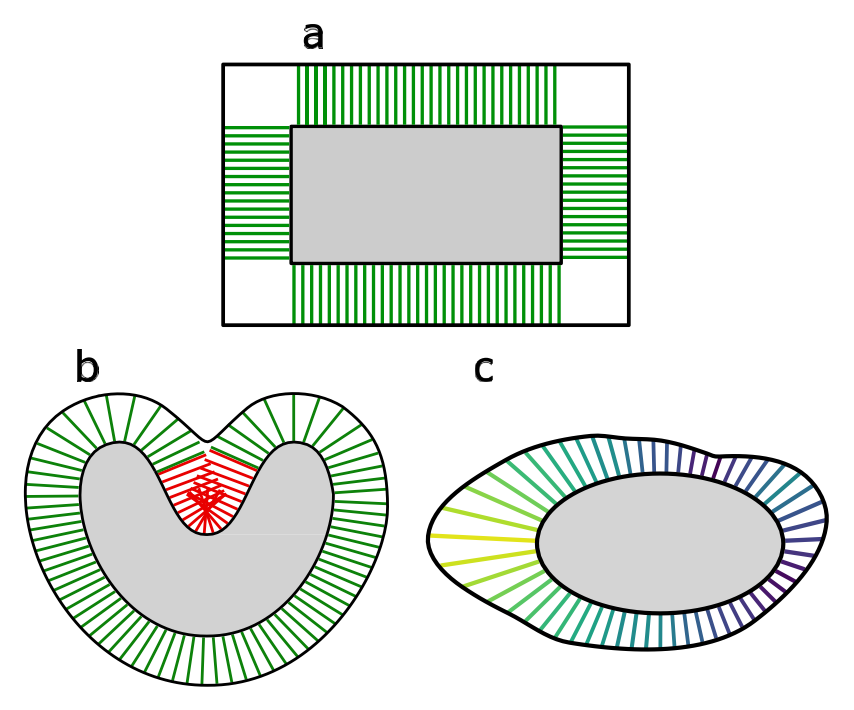


Figure 5. Some cartoons illustrating scenarios where our model breaks down. (a) Shape with sharp corners that a molecule will not fill effectively; (b) deep, sharp "cut" causing the shell to have overlapping volume; and (c) generally nonuniform shell.

particle itself. We have thus demonstrated that the assumptions of dynamic light scattering are inherently more accurate than one would otherwise assume, although we stress that this finding does have limits. As an extreme example, while it is true that the shape of a carbon nanotube and its associated solvation shell is more spherical than the carbon nanotube itself, the composite of the nanotube and its solvation shell is still extremely nonspherical. These findings also guarantee that the coatings on a particle, whether this is a true core/shell construction, the capping agent of a nanoparticle, the brushes on a brush polymer, or even the surfactant in a micelle or reverse micelle, will make the spherical particle assumption of the Stokes—Einstein equation of a spherical particle more correct as the shell becomes larger.

Our proof is purely geometric and, therefore, does not consider whether the core/shell construction is positive space composed of matter or negative space defined by the absence of matter. Therefore, our findings work equally well within a pore or cavity. That is, we predict that removing a constant thickness shell within an arbitrary cavity will result in a more spherical cavity. Mean curvature is an extensive property dependent on the size of the object, so scaling an object up will lower the mean curvature. However, our work implies that the mean curvature of the surface of such a cavity would decrease more than would be expected by simply scaling the original shape. This suggests that, for example, the sorption properties and sorption-induced deformation of porous materials may be more closely linked to the pore size distribution than previously assumed. 64

The contrapositive statement of our proof is also true, so that if we reduce all measures of shape for an arbitrary shape by some constant amount, t, such as by etching away the shell of a nanoparticle, then assuming that the moments of inertia do not begin exactly equal to each other, e.g., assuming the original particle is not exactly spherical, the CPE must rise, and the shape must become less spherical. Stated another way, removing material from a shape will amplify whatever irregularities were

initially present. Shortening the tail groups on a micelle can, therefore, be expected to amplify whatever nonspherical irregularities were present relative to their longer-tailed cousins. In another context, this suggests that if something like an arbitrary sand particle is uniformly eroded, it is more likely than not that the particle will become less spherical and that if the particle becomes more spherical, then we can conclude that the erosion was nonuniform.

We note that our model is based on extremely simple geometric objects, while chemical systems are often far more complex. Our model predicts that the change in CPE depicted in Figure 4 for a real reverse micelle should always appear in the third quadrant, and indeed, the majority of our data do fall within this quadrant. However, not all of the data appear in the third quadrant. We propose that the relative portion of real data that behaves as predicted by our model can be used as a measure of how well a given chemical system is modeled. That is, 67% of the time, the difference between the CPE of the outer and inner surfaces of our simulated AOT reverse micelles lies in the third quadrant. This implies that 67% of the time, they behave as simple, geometric core/shell constructs. However, Figure 4 clearly shows density present in all four quadrants, even if it occurs in only a minority of cases. So, there are times when our model breaks down and does not describe real systems.

Our model makes numerous simplifying assumptions to predict behavior that may not be true for real systems. For example, the system must have a completely uniform thickness in its shell, adding precisely equally to each measure of shape. The shape must be one of the limited set of shapes that have analytical, linear equations to describe their moments of inertia, which are also topological balls. However, real chemical systems are not perfect. A nanoparticle may be modeled as an ellipsoid to a first approximation but is never perfectly ellipsoidal, if for no other reason than it comprises a crystal lattice with discrete numbers of atoms introducing steps in places rather than a smooth surface. A micelle may also be spherical on average but is

not perfectly spherical at any given point in time. Additionally, while our model is predicated on the addition of a constant thickness to all measurements of shape, this might not be achieved in practice. In the case of a reverse micelle, the surfactant layer adds thickness to the particle, but to be perfectly equal in all directions, each surfactant molecule must be exactly oriented along a local surface normal and be exactly equally arranged, and all adopt the exact same conformation so that they are exactly the same length at all points on the surface at all times. This very strict list of conditions is virtually never attainable in real systems.

We have identified three broad classes where the assumptions of our model break down, as illustrated in Figure 5. In Figure 5a, we depict a shape with sharp corners that are not populated by the chemical that creates the shell. Most likely, this would be encountered as a relative bald spot on an object with some surfactant layer. Note that this situation only works for certain systems. For example, a noble metal shell grown on a metallic, cubic nanoparticle will typically fill the corner easily enough. But surfactants around a cubic nanoparticle might encounter this problem. Ultimately, this results in a nonuniform distribution of the shell that violates the construction of our model.

In Figure 5b, we consider a shape that has a deep cut or crease in the shape, where addition of a constant thickness around the shape results in overlap in the vicinity of the crease, highlighted in red. We have identified this situation in our own reverse micelle simulation. Matter cannot overlap, as shown in Figure 5b, and so the tail groups of the reverse micelle instead push against each other and "fill in" the crease. In this way, the outer surface is not increased by a constant amount, so the model proposed here does not hold true. More generally, if the shell overlaps with itself, then the volume can only be filled once, and the shell is no longer geometrically similar to the core.

In Figure 5c, we illustrate the case where the shell is simply nonuniform for any number of reasons. For example, this may occur when the tail groups of a capping agent adopt varying conformations at distinct points on the surface, so that the effective length of the capping agent layer is uneven. For example, if the circular cap of the cylinder in Figure 3 were chemically distinct from the curved sides, such that a surfactant tended to extend along the circular cap but lie flat along the curved sides, the shell layer would be nonuniform. Alternatively, this situation could happen if the growth of a nanoparticle shell is chaotic and uneven.

Although we know that our model does not apply in these situations, this does not automatically mean that the CPE rises instead of falling. In general, we note that the moments of inertia must increase because the shell is necessarily larger than the core, but that is the only restriction. So long as the moments of inertia grow, it is equally probable for the A moment of inertia to grow the most or the least, and so on. Therefore, our model is really a special subset of the possible changes in CPE. Within this subset, behavior is predictable, and we can guarantee that CPE falls, but outside of that subset, the CPE could rise, it could fall, it could remain the same, or any combination of the three between the two axes of CPE: e_{ab} and e_{ac} . For example, as drawn, Figure 5b shows a "U"-shaped inner surface and a heart-shaped outer surface. If we continued this pattern, the outer surface would eventually become circular, and so as drawn, this situation indicates a drop in the CPE (technically, a drop in the 2D analogue of CPE: eccentricity). On the other hand, Figure 5c shows greater "hair" length along the long axis of the shape, while the short axis has shorter hairs, making the outer surface

significantly less circular than the inner surface, a situation not unlike a bicelle assembly. Therefore, the situation as drawn would indicate a rise in the CPE. If we were to instead have the longer "hairs" along the short axis and the shorter hairs along the long axis, then the CPE would fall, in the short term, before rising if the pattern were continued.

Absent some chemical reason unique to a particular system of interest, it is equally likely for a crease or uneven "hairs" (e.g., surfactant molecules, metal shell thickness, etc.) to develop on any side of a shape, making it equally likely for these irregularities to cause either a rise or a fall in the CPE. Therefore, the change in CPE for a shape that is not well described by our model should be expected to be uniformly distributed across all four quadrants and about the origin. This concept allows us to analyze the distribution that we observed in our own simulations, shown in Figure 4, in more detail. In the instance where our simulation is not well modeled, the most common scenario is for e_{ab} to rise while e_{ac} falls, as indicated by the horizontal skew in the data in Figure 4. The distributions between the first, second, and fourth quadrants should be roughly equal unless there is a chemical reason for the difference, so we conclude that there exists a chemical reason for this observation. The situation where Δe_{ab} > 0 while Δe_{ac} < 0 could be explained by a number of different situations. For example, the smallest semiaxis, c, grows faster than the largest semiaxis, a, while the middle semiaxis, b, grows more slowly than a (i.e., $\delta c > \delta a > \delta b$). This could be caused by a crease in the direction of b, as in Figure 5b, or by the surfactant tails being apparently shorter in the direction of b, presumably due to the surfactant tails lying relatively flat in this direction, as in Figure 5c. Other scenarios could also account for the behavior depicted in Figure 4. A full analysis of the shape of AOT reverse micelles is beyond the scope of this paper and will be examined in a future paper.

5. CONCLUSIONS

We have created a mathematical model for core/shell structures and proven how the shell impacts the shape of the object. This purely geometric model grants us broad insight into the behavior of the ubiquitous core/shell motif, allowing us to make broadly applicable states across both simulation and experiment for a broad range of seemingly disconnected chemical systems, ranging from solution dynamics and thermodynamics to nanoparticles to porous materials and beyond. In addition, this broad geometric understanding allows us to separate out expected effects due to geometry from unexpected effects due to chemistry that could not otherwise be identified. We demonstrate this work on simulated AOT reverse micelles and show that even though the model is very simple, it is surprisingly effective at modeling even the highly irregular and amorphous reverse micelles. This model also allowed us to identify that AOT reverse micelles exhibit anomalous behavior that cannot be understood by geometry alone. This suggests that among the many complex interactions within the reverse micelle, there is some sort of consistent interaction giving rise to this behavior that would have been impossible to identify otherwise.

ASSOCIATED CONTENT

Solution Supporting Information

The Supporting Information is available free of charge at https://pubs.acs.org/doi/10.1021/acs.jpcb.3c07652.

The reverse micelle's apparent semiaxes over time, used to generate the data presented here, are presented as a TXT

file with the SI. The numbers are given in the order: simulation time (ps), inner surface e_{ab} and e_{ac} , outer surface e_{ab} and e_{ac} . Appendix (TXT)

The proof underlying this work is presented in the SI Appendix (PDF)

AUTHOR INFORMATION

Corresponding Authors

Christopher D. Gale — Department of Chemistry, Colorado State University, Fort Collins, Colorado 80523, United States; orcid.org/0000-0002-2661-484X; Email: cgale@colostate.edu

Nancy E. Levinger — Department of Chemistry, Colorado State University, Fort Collins, Colorado 80523, United States; orcid.org/0000-0001-9624-4867;

Email: Nancy.Levinger@colostate.edu

Complete contact information is available at: https://pubs.acs.org/10.1021/acs.jpcb.3c07652

Notes

The authors declare no competing financial interest.

ACKNOWLEDGMENTS

The authors gratefully acknowledge financial support from Colorado State University and NSF CHE 1956323. This work utilized the resources from the University of Colorado Boulder Research Computing Group, which is supported by the National Science Foundation (awards ACI-1532235 and ACI-1532236), the University of Colorado Boulder, and Colorado State University. The authors would like to thank Drs. Alexander Hulpke and Grzegorz Szamel as well as Donald Minford, M.E.A., for reviewing the proof underlying this work and their exceptionally helpful comments.

REFERENCES

- (1) Chatterjee, K.; Sarkar, S.; Rao, K. J.; Paria, S. Core/shell nanoparticles in biomedical applications. *Adv. Colloid Interface Sci.* **2014**, 209, 8–39.
- (2) Gawande, M. B.; Goswami, A.; Asefa, T.; Guo, H.; Biradar, A. V.; Peng, D. L.; Zbo- ril, R.; Varma, R. S. Core-shell nanoparticles: synthesis and applications in catalysis and electrocatalysis. *Chem. Soc. Rev.* **2015**, *44*, 7540–7590.
- (3) Chen, X.; Peng, D.; Ju, Q.; Wang, F. Photon upconversion in coreshell nanoparticles. *Chem. Soc. Rev.* **2015**, *44*, 1318–1330.
- (4) Ferrando, R. Symmetry breaking and morphological instabilities in core-shell metallic nanoparticles. *J. Condens. Matter Phys.* **2015**, *27*, 013003 DOI: 10.1088/0953-8984/27/1/013003.
- (5) Haag, R. Supramolecular Drug-Delivery Systems Based on Polymeric Core-Shell Architectures. *Angew. Chem., Int. Ed. Engl.* **2004**, 43, 278–282.
- (6) Lu, W.; Guo, X.; Luo, Y.; Li, Q.; Zhu, R.; Pang, H. Core-shell materials for advanced batteries. *Chem. Eng. J.* 2019, 355, 208–237.
- (7) Levinger, N. E. Water in confinement. *Science* **2002**, 298, 1722–1723.
- (8) Piletic, I. R.; Moilanen, D. E.; Spry, D. B.; Levinger, N. E.; Payer, M. D. Testing the core/shell model of nanoconfined water in reverse micelles using linear and nonlinear IR spectroscopy. *J. Phys. Chem. A* **2006**, *110*, 4985–4999.
- (9) Ansari, N.; Laio, A.; Hassanali, A. Spontaneously Forming Dendritic Voids in Liquid Water Can Host Small Polymers. *J. Phys. Chem. Lett.* **2019**, *10*, 5585–5591.
- (10) Basilevsky, M. V.; Parsons, D. F. An advanced continuum medium model for treating solvation effects: Nonlocal electrostatics with a cavity. *J. Chem. Phys.* **1996**, *105*, 3734–3746.

- (11) Li, L.; Li, C.; Zhang, Z.; Alexov, E. On the dielectric "constant" of proteins: Smooth dielectric function for macromolecular modeling and its implementation in DelPhi. *J. Chem. Theory Comput.* **2013**, *9*, 2126–2136.
- (12) Lake, P. T.; Mattson, M. A.; McCullagh, M. Implicit Solvation Using the Superposition Approximation (IS-SPA): Extension to Peptides in a Polar Solvent. *J. Chem. Theory Comput.* **2021**, *17*, 703–713.
- (13) Zemke, J. M.; Franz, J. A Biphasic Ligand Exchange Reaction on CdSe Nanoparticles: Introducing Undergraduates to Functionalizing Nanoparticles for Solar Cells. *J. Chem. Educ.* **2016**, *93*, 747–752.
- (14) Chu, Z.; Dreiss, C. A.; Feng, Y. Smart wormlike micelles. *Chem. Soc. Rev.* **2013**, *42*, 7174–7203.
- (15) Lu, Y.; Zhang, E.; Yang, J.; Cao, Z. Strategies to improve micelle stability for drug delivery. *Nano Res.* **2018**, *11*, 4985–4998.
- (16) Wubshet, N. H.; Liu, A. P. Methods to mechanically perturb and characterize GUV- based minimal cell models. *Comput. Struct. Biotechnol. J.* **2023**, 21, 550–562.
- (17) Hvidsten, T. R.; Lægreid, A.; Kryshtafovych, A.; Anderson, G.; Fidelis, K.; Komorowski, J. A comprehensive analysis of the structure-function relationship in proteins based on local structure similarity. *PLoS One* **2009**, *4*, 06266 DOI: 10.1371/journal.pone.0006266.
- (18) Mabrouk, M.; Hammad, S. F.; Abdella, A. A.; Mansour, F. R. Tips and tricks for successful preparation of molecularly imprinted polymers for analytical applications: A critical review. *Microchem. J.* **2023**, *193*, No. 109152.
- (19) Resina, L.; Alemán, C.; Ferreira, F. C.; Esteves, T. Protein-imprinted polymers: How far have "plastic antibodies" come? *Biotechnol. Adv.* **2023**, *68*, No. 108220.
- (20) Klein, W. P.; Schmidt, C. N.; Rapp, B.; Takabayashi, S.; Knowlton, W. B.; Lee, J.; Yurke, B.; Hughes, W. L.; Graugnard, E.; Kuang, W. Multiscaffold DNA origami nanoparticle waveguides. *Nano Lett.* **2013**, *13*, 3850–3856.
- (21) Parsons, M. F.; Allan, M. F.; Li, S.; Shepherd, T. R.; Ratanalert, S.; Zhang, K.; Pullen, K. M.; Chiu, W.; Rouskin, S.; Bathe, M. 3D RNA-scaffolded wireframe origami. *Nat. Commun.* **2023**, *14*, No. 382.
- (22) Flor, B.; Zeman, C. J.; Ma, X.; Schatz, G. C. Wavelength-Dependent Spin Excitation with Circularly Polarized Light in CdSe Nanoplatelets. *J. Phys. Chem. C* **2023**, *127*, 14317–14325.
- (23) Vargas-Consuelos, C. I.; Camacho-López, M. A.; Ramos-Sanchez, V. H.; Graeve, O. A. Phase and Morphology Control of Hexagonal MoO₃ Crystals via Na⁺ Interactions: A Raman Spectroscopy Study. *J. Phys. Chem. C* **2023**, *127*, 13136–13148.
- (24) Qiao, S.; Novitskaya, E.; Ren, T.; Pena, G.; Graeve, O. A. Phase and Morphology Control of Magnesium Nanoparticles via Lithium Doping. *Cryst. Growth Des.* **2019**, *19*, 3626–3632.
- (25) Ren, T.; Tran, R.; Lee, S.; Bandera, A.; Herrera, M.; Li, X. G.; Ong, S. P.; Graeve, O. A. Morphology Control of Tantalum Carbide Nanoparticles through Dopant Additions. *J. Phys. Chem. C* **2021**, *125*, 10665–10675.
- (26) Schönfeldová, T.; Dupertuis, N.; Chen, Y.; Ansari, N.; Poli, E.; Wilkins, D. M.; Hassanali, A.; Roke, S. Charge Gradients around Dendritic Voids Cause Nanoscale Inhomogeneities in Liquid Water. *J. Phys. Chem. Lett.* **2022**, *13*, 7462–7468.
- (27) Mizuta, K.; Ishii, Y.; Kim, K.; Matubayasi, N. Bridging the gap between molecular dynamics and hydrodynamics in nanoscale Brownian motions. *Soft Matter* **2019**, *15*, 4380–4390.
- (28) Choi, S.; Cheung, C.; Graeve, O. A. Fabrication of continuous linear pores in an SOFC anode using unidirectional carbon fibers as sacrificial templates. *J. Am. Ceram.* **2021**, *104*, 3030–3041.
- (29) Alberts, B.; Johnson, A.; Lewis, J.; Raff, M.; Roberts, K.; Walter, P. *Mol. Biol. Cell*, 4; Garland Science: New York, 2002, Chapter 8.
- (30) Vedel, I. M.; Papagiannoula, A.; Naudi-Fabra, S.; Milles, S. Nuclear magnetic resonance/single molecule fluorescence combinations to study dynamic protein systems. *Curr. Opin. Struct. Biol.* **2023**, 82, No. 102659.
- (31) Lata, K.; Charles, S.; Mangala Prasad, V. Advances in computational approaches to structure determination of alphaviruses

- and flaviviruses using cryo-electron microscopy. J. Struct. Biol. 2023, 215, No. 107993.
- (32) Boresch, S.; Ringhofer, S.; Höchtl, P.; Steinhauser, O. Towards a better description and understanding of biomolecular solvation. *Biophys. Chem.* **1999**, *78*, 43–68.
- (33) Gale, C. D.; Derakhshani-Molayousefi, M.; Levinger, N. E. How to Characterize Amorphous Shapes: The Tale of a Reverse Micelle. *J. Phys. Chem. B* **2022**, *126*, 953–963.
- (34) Abel, S.; Sterpone, F.; Bandyopadhyay, S.; Marchi, M. Molecular modeling and simulations of AOT-water reverse micelles in isooctane: Structural and dynamic properties. *J. Phys. Chem. B* **2004**, *108*, 19458–19466.
- (35) Mudzhikova, G. V.; Brodskaya, E. N. Molecular simulation of an aerosol OT reverse micelle: 1. the shape and structure of a micelle. *Colloid J.* **2006**, *68*, 729–737.
- (36) Chowdhary, J.; Ladanyi, B. M. Molecular dynamics simulation of aerosol-OT reverse micelles. *J. Phys. Chem. B* **2009**, *113*, 15029–15039.
- (37) Martinez, A. V.; Dominguez, L.; Małolepsza, E.; Moser, A.; Ziegler, Z.; Straub, J. E. Probing the structure and dynamics of confined water in AOT reverse micelles. *J. Phys. Chem. B* **2013**, *117*, 7345–7351.
- (38) Willard, A. P.; Chandler, D. Instantaneous liquid interfaces. J. Phys. Chem. B 2010, 114, 1954–1958.
- (39) Sega, M.; Hantal, G.; Fábián, B.; Jedlovszky, P. Pytim: A Python package for the interfacial analysis of molecular simulations. *J. Comput. Chem.* **2018**, *39*, 2118–2125.
- (40) Du, C.; He, W.; Yin, T.; Shen, W. Volumetric properties of water/AOT/isooctane microemulsions. *Langmuir* **2014**, *30*, 15135–15142.
- (41) Bussi, G.; Donadio, D.; Parrinello, M. Canonical sampling through velocity rescaling. *J. Chem. Phys.* **2007**, *126*, 014101 DOI: 10.1063/1.2408420.
- (42) Berendsen, H. J. C.; Postma, J. P.; Van Gunsteren, W. F.; Dinola, A.; Haak, J. R. Molecular dynamics with coupling to an external bath. *J. Chem. Phys.* **1984**, *81*, 3684–3690.
- (43) Hoover, W. G. Canonical dynamics: Equilibrium phase-space distribution. *Phys. Rev. A* **1985**, *31*, 1695–1697.
- (44) Nosé, S. A molecular dynamics method for simulations in the canonical ensemble. *Mol. Phys.* **2002**, *100*, 191–198.
- (45) Parrinello, M.; Rahman, A. Polymorphic transitions in single crystals: a new molecular dynamics method. *J. Appl. Phys.* **1981**, *52*, 7182–7190.
- (46) Nosé, S.; Klein, M. Constant pressure molecular dynamics for molecular systems. *Mol. Phys.* **1983**, *50*, 1055–1076.
- (47) Jorgensen, W. L.; Chandrasekhar, J.; Madura, J. D.; Impey, R. W.; Klein, M. L. Comparison of simple potential functions for simulating liquid water. *J. Chem. Phys.* **1983**, *79*, 926–935.
- (48) Klauda, J. B.; Venable, R. M.; Freites, J. A.; O'Connor, J. W.; Tobias, D. J.; Mondragon-Ramirez, C.; Vorobyov, I.; MacKerell, A. D.; Pastor, R. W. Update of the CHARMM all-atom additive force field for lipids: Validation on six lipid types. *J. Phys. Chem. B* **2010**, *114*, 7830–7843.
- (49) Berendsen, H. J.; van der Spoel, D.; van Drunen, R. GROMACS: A message-passing parallel molecular dynamics implementation. *Comput. Phys. Commun.* **1995**, *91*, 43–56.
- (50) Van Der Spoel, D.; Lindahl, E.; Hess, B.; Groenhof, G.; Mark, A. E.; Berendsen, H. J. GROMACS: Fast, flexible, and free. *J. Comput. Chem.* **2005**, *26*, 1701–1718.
- (51) Martínez, L.; Andrade, R.; Birgin, E. G.; Martínez, J. M. PACKMOL: A package for building initial configurations for molecular dynamics simulations. *J. Comput. Chem.* **2009**, *30*, 2157–2164.
- (52) Abraham, M. J.; Murtola, T.; Schulz, R.; Páll, S.; Smith, J. C.; Hess, B.; Lindah, E. GROMACS: High performance molecular simulations through multi-level parallelism from laptops to supercomputers. *SoftwareX* **2015**, *1*–2, 19–25.
- (53) Theodorou, D. N.; Suter, U. W. Shape of Unperturbed Linear Polymers: Polypropylene. *Macromolecules* **1985**, *18*, 1206–1214.
- (54) Gregorová, E.; Pabst, W.; Vaněrková, L. Anisometric Particle Systems from Shape Characterization to Suspension Rheology, AIP Conf. Proc., 2009; pp 1027–1030.

- (55) Siddiqi, A.; Herdes, C. Water effect in the reverse micellar formation of docusate sodium. A coarse-grained molecular dynamics approach. *Fluid Phase Equilibria* **2022**, *559*, No. 113469.
- (56) Rawat, N.; Biswas, P. Size, shape, and flexibility of proteins and DNA. J. Chem. Phys. **2009**, 131, 165104–165113.
- (57) Skiena, S. S. The Algorithm Design Manual, Springer-Vrlag: New York, 1997; Chapter 8.6, pp 395–396.
- (58) Boukouvala, C.; Daniel, J.; Ringe, E. Approaches to modelling the shape of nanocrystals. *Nano Converg* **2021**, *8*, 26 DOI: 10.1186/s40580-021-00275-6.
- (59) Stetefeld, J.; McKenna, S. A.; Patel, T. R. Dynamic light scattering: A practical guide and applications in biomedical sciences. *Biophys. Rev.* **2016**, *8*, 409–427.
- (60) Bhattacharjee, S. DLS and zeta potential What they are and what they are not? *J. Controlled Release* **2016**, 235, 337–351.
- (61) Edward, J. T. Molecular volumes and the Stokes-Einstein equation. *J. Chem. Educ.* **1970**, 47, 261–270.
- (62) Hassan, P. A.; Rana, S.; Verma, G. Making sense of Brownian motion: Colloid characterization by dynamic light scattering. *Langmuir* **2015**, 31, 3–12.
- (63) Ausman, K. D.; O'Connell, M. J.; Boul, P.; Ericson, L. M.; Casavant, M. J.; Walters, D. A.; Huffman, C.; Saini, R.; Wang, Y.; Haroz, E.; Billups, E. W.; Smalley, R. E. In *Roping and Wrapping Carbon Nanotubes*, AIP Conference Proceedings 591, 2001, pp 226–230.
- (64) Eskandari-Ghadi, M.; Zhang, Y. Effect of pore size distribution on sorption-induced deformation of porous materials: A theoretical study. *Int. J. Solids Struct.* **2022**, 242, No. 111533.